Mineralization of Calcium Phosphate Crystals in Starch Template Inducing a Brushite Kidney Stone Biomimetic Composite

ARTICLE *in* CRYSTAL GROWTH & DESIGN · MARCH 2013

Impact Factor: 4.89 · DOI: 10.1021/cg4002434

4 AUTHORS, INCLUDING:

Mazeyar Parvinzadeh Gashti
McGill University
85 PUBLICATIONS **909** CITATIONS

CRYSTAL GROWTH & DESIGN

Article

pubs.acs.org/crystal

Mineralization of Calcium Phosphate Crystals in Starch Template Inducing a Brushite Kidney Stone Biomimetic Composite

Mazeyar Parvinzadeh Gashti,*[,†,‡] Manuela Stir,[†] Marc Bourquin,[†] and Jürg Hulliger*[,†]

[†]Department of Chemistry & Biochemistry, University of Berne, Freiestrasse 3 CH-3012 Berne, Switzerland

[‡]Department of Textile, Islamic Azad University, Shahre Rey Branch, Tehran, Iran

ABSTRACT: Dicalcium phosphate dihydrate (brushite) and octacalcium phosphate (OCP) crystals are precursors of hydroxyapatite (HAp) for tooth enamel, dentine, and bones formation in living organisms. Here, we introduce a new method for biomimicking brushite and OCP in starch using single and double diffusion techniques. Brushite and OCP crystals were grown by precipitation in starch after gelation. The obtained materials were analyzed by infrared spectroscopy (IR), scanning electron microscopy (SEM), X-ray diffraction (XRD), and confocal laser scanning microscopy (CLSM). IR spectra demonstrate starch inclusion by peak shifts in the 2900−3500 cm^{-1} region. SEM showed two different morphologies: plate-shaped and needle-like crystals. Calcium phosphate/starch aggregates bear strong resemblance to prismatic brushite kidney stones. This may open up a clue to understand the mechanism of kidney stone formation.

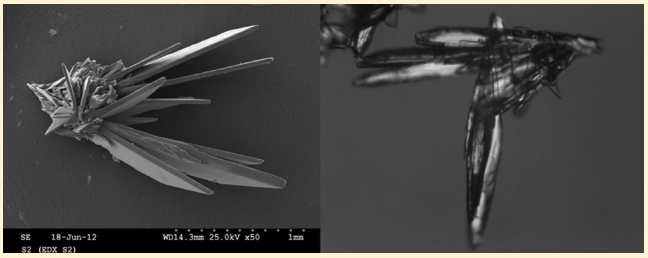

INTRODUCTION

Starch is a family of water-soluble linear polysaccharides composed of a number of monosaccharides or sugar (glucose) molecules joined together with α-D-(1−4) and/or α-D-(1−6) linkages.[1] It consists of two types of molecules, the linear and helicalamylose, typically constituting 15 to 20% of starch, and the branched amylopectin, which is the major component.[2] The hydroxyl groups on the glucose units are responsible for its anionic polarity.[3] Starch is widely used as an additive in food, papermaking, and textile industries. It is used in food products as a thickener and stabilizer. It is also used in nonfood industries as an adhesive for papermaking and as a sizing agent to reduce the breaking of cotton based yarns during weaving.[4]

Brushite ($CaHPO_4{\cdot}2H_2O$) and OCP ($Ca_8H_2(PO_4)_6{\cdot}5H_2O$) are two main calcium-containing bioceramics, which have generally been of special interest to tissue engineering scientists due to their biocompatibility, osteoconductivity, porous ability, surface charge density, functionality, self-setting property, injectability, bioactivity, unique formability, and less degradability compared to other bioceramics.[5−7] Brushite and OCP crystals can be grown in gels for a demonstration of mechanisms of mineral formation in calcified tissues and crystal deposition diseases.[8,9] Gels made of polar or nonpolar polymers may act as a template to induce nucleation of crystals to understand in vivo mineralization in tissues.[10] So far, brushite and OCP were mostly produced in silica gel.[11−16] Iafisco et al.[16] showed that the precipitation of calcium phosphates can be controlled by calcium chloride diffusion through silica gel prepared at different densities. Furuichi et al.[17] produced nanofibrous HAp ($Ca_{10}H_2(PO_4)_6(OH)_2$) through dehydration of brushite in gelatin. We have recently demonstrated that incorporation of glutamic acid in gelatin creates a new level of network for mineralization of mushroom-like brushite. Such a composite bears a strong resemblance to the brushite kidney stones stating a prominent role of glutamic acid in kidney stone formation.[18]

Former works on crystal growth in starch are focused on the effects of a gel on crystallization of porous bioactive calcium carbonate and HAp scaffolds.[19−22] More recently, biomimetic preparation of HAp biocomposites was performed in pure starch gel,[23,24] starch/gelatin,[25,26] and starch/*N*-vinylpyrrolidone mixtures via microwave vacuum drying and γ-radiation induced graft copolymerization techniques.[27] However, none of these studies focused on synthesizing brushite and OCP crystals in starch gel.

EXPERIMENTAL SECTION

The procedure used to synthesize brushite and OCP crystals consisted of preparing a 20% w/w starch gel in water (catalog no. 1252; Merck HGaA, Darmstadt, Germany) and buffered solutions for several single- and double-diffusion experiments. Table 1 shows the set of experiments for sample preparation. For single tube 1, starch was dissolved in deionized water, and then, 7 cc of $CaCl_2$ solution was added to the gel, adjusting the pH with 2 N HCl to maintain a value of 4.5. The tube was left at room temperature for 24 h until gelation had occurred. Then, 7 cc of Na_2HPO_4 solution (buffered at pH 7.4) was poured onto the starch gel to effect diffusion at 25 °C for 3 weeks. Alternatively, starch was mixed with Na_2HPO_4 solution to gel in contact with $CaCl_2$ solution (single tube 2). For the double-diffusion method, U-tubes (vertical section, 20 cm; horizontal section, 12 cm; diameter, 2 cm) were filled with acidified starch at pH 4.5. Buffered $CaCl_2$ and Na_2HPO_4 solutions were filled in both sides of the tubes.

Received: February 12, 2013
Revised: March 15, 2013
Published: March 18, 2013

dx.doi.org/10.1021/cg4002434 | *Cryst. Growth Des.* 2013, 13, 2166−2173

Table 1. Set of Experiments Used in This Study

sample tube	method	molarity of $CaCl_2$	molarity of Na_2HPO_4	molar ratio of Ca/P	type of crystal in the tube
1	single diffusion	0.19	0.12	1.58	brushite
2	single diffusion	0.19	0.12	1.58	brushite
3	double diffusion	1	1.8	0.55	brushite
4	double diffusion	1	0.8	1.25	brushite + OCP
5	double diffusion	0.2	0.2	1	brushite + OCP

After 3 weeks, brushite and OCP particles were collected and washed several times with hot water to remove excess gel and dried at 80 °C. The experiments were repeated for each set of samples in 10 tubes.

Chemical characterization of starch and crystals was carried out using a Perkin-Elmer Spectrum One IR spectrometer.

Surface morphology analysis was carried out using a Hitachi scanning electron microscope S-3000 N. Samples were coated with an Au layer under vacuum conditions prior to the measurement. The presence of calcium and phosphate on the crystal surface was determined by a Noran SIX NSS200 energy dispersive X-ray detector (EDX) attached to the SEM.

Powder X-ray diffraction patterns were collected at ambient temperature using a STOE StadiP diffractometer in transmission Debye–Scherrer geometry (monochromatic Cu $K\alpha_1$ radiation, wavelength λ = 0.15406 nm). Specimens were filled to 0.5 mm capillaries. The scattered intensity was detected by using a one-dimensional curved position sensitive detector (linear PSD). The diffractometer goniometer radius equals 130 mm. Crystallite (grain) sizes G were evaluated using the Scherrer equation

$$G_{hkl} = \frac{K\lambda}{\beta \cos \theta_{hkl}} \quad (1)$$

where K is the shape constant (here, K = 1), λ is the X-ray wavelength (here, λ = 0.15406 nm, Cu K_α radiation), β is the full-width at half-maximum (fwhm, in radians), and θ_{hkl} is the Bragg angle of the diffraction line having Miller indices (hkl).

The distribution of starch in brushite was investigated using a confocal laser scanning microscope (Zeiss LSM 510 Meta, Axiovert 200M). Two parts per million of a biological fluorescent dye (pyranine) was dissolved in starch for a U-tube, and stained crystals were collected.

RESULTS AND DISCUSSION

Chemical Characterization. The IR spectra of starch, pure brushite, and calcium phosphate crystals prepared in starch gel are shown in Figures 1 and 2. The angular deformation of C–H bonds in starch is reflected by two bands at 1468 and 1380 cm^{-1}. The characteristic band at 984 cm^{-1} along with the peaks at 1082 and 1160 cm^{-1} are assigned to the C–C, C–O–H, and C–O–C stretching vibrations of the pyranose ring in the solid starch, respectively.[4] The skeleton bending of pyranose ring is known to appear at 708 and 763 cm^{-1}. Other bands at 1637, 2921, and 3435 cm^{-1} are related to adsorbed water molecules, asymmetric C–H stretching, and O–H stretching vibration in starch.[28]

Analytical grade of brushite supplied by Sigma-Aldrich was compared with calcium phoshphate/starch composite crystals obtained in this study (Figure 1b). It is evident that the O–H stretching of water molecules appears at 3544, 3487, 3278, and 3165 cm^{-1} as two intense and two shoulder peaks.[29,30] The bands at 2384 and 1649 cm^{-1} are assigned to O–H stretching of the hydrogen phosphate anions and bending of H_2O molecules, respectively.[31−34] Another band at 1209 cm^{-1} in the calcium phosphate is assigned to in-plane P–O–H bending. The PO stretches are mainly characterized in the PO_4^{-3} fragment by three strong bands at 1137, 1064, and 986 cm^{-1}. The P–O(H) stretching and liberation of H_2O molecules gives rise to two bands at 874 and 793 cm^{-1}, respectively. The bands at 660, 577, and 526 cm^{-1} were assigned to P–O bending of the PO_4^{-3} fragment.[35,36]

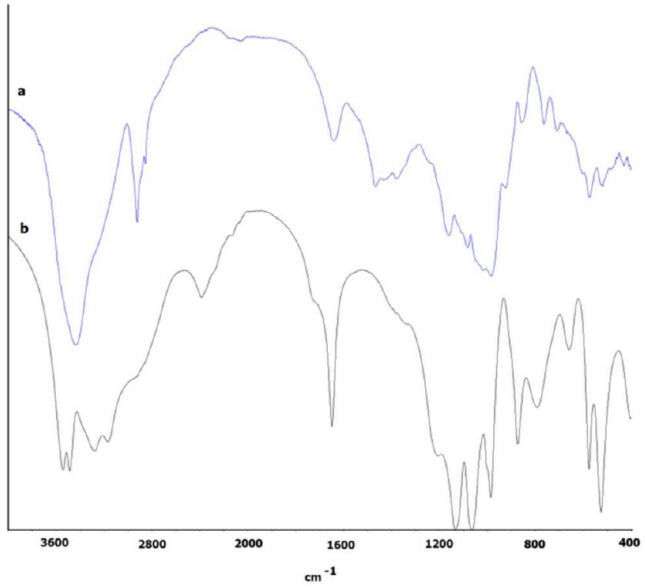

Figure 1. IR spectra of (a) starch and (b) analytical grade brushite (Sigma-Aldrich).

As seen in Figure 2a, after the crystallization of calcium phosphate in 20% starch, a new peak appeared at 2922 cm^{-1}, and the band at 2384 cm^{-1} shifted to 2377 cm^{-1}. The spectral data (Figure 2b) shows the appearance of a new peak at 2919 cm^{-1} and the shift of the peaks at 3288 and 1214 cm^{-1}. These changes, also observed in Figure 2c, are due to hydrogen bonding between starch and calcium phosphate crystals.[23,24] Besides, the bands at 3278, 1137, 1064, and 660 cm^{-1} shifted to 3291, 1127, 1054, and 654 cm^{-1} (Figure 2d) compared to pure brushite. Similar peak shifts were observed in Figure 2e, supporting reports by Xiang et al.[21] and Sadjadi et al.[23] The latter authors showed that the formation of hydrogen bonds between starch and calcium carbonate or HAp leads to a shift of IR peaks in the 2900–3500 cm^{-1} region as a result of starch incorporation in the lattice structure.

The IR spectrum for calcium phosphate crystals prepared in tube 2 (Figure 2b) are almost the same as those in tube 1 (Figure 2a). An exception is the shift of the O–H vibrations at 3288 and 3162 cm^{-1} compared to crystals in tube 1. This can be due to changes of hydrogen bonds between OH groups of starch and calcium phosphate crystals.[21,23] The incorporation of more phosphate ions (as proven by EDX) in the crystals produced in tube 3 by double-diffusion resulted in the shift of the IR peaks at 3284, 1136, and 662 cm^{-1}. This is due to P–O stretching and bending vibrations.[37]

Surface Morphology by SEM. Microcrystals and plate-shaped morphologies arranged in clusters were obtained by single-tube diffusion in tubes 1 and 2 (Figure 3a–e). Microscale units of such crystals with 1000 μm width are the building blocks of 3D composite superstructures. The SEM images reveal that separate microplatelets originate from a common

dx.doi.org/10.1021/cg4002434 | Cryst. Growth Des. 2013, 13, 2166–2173

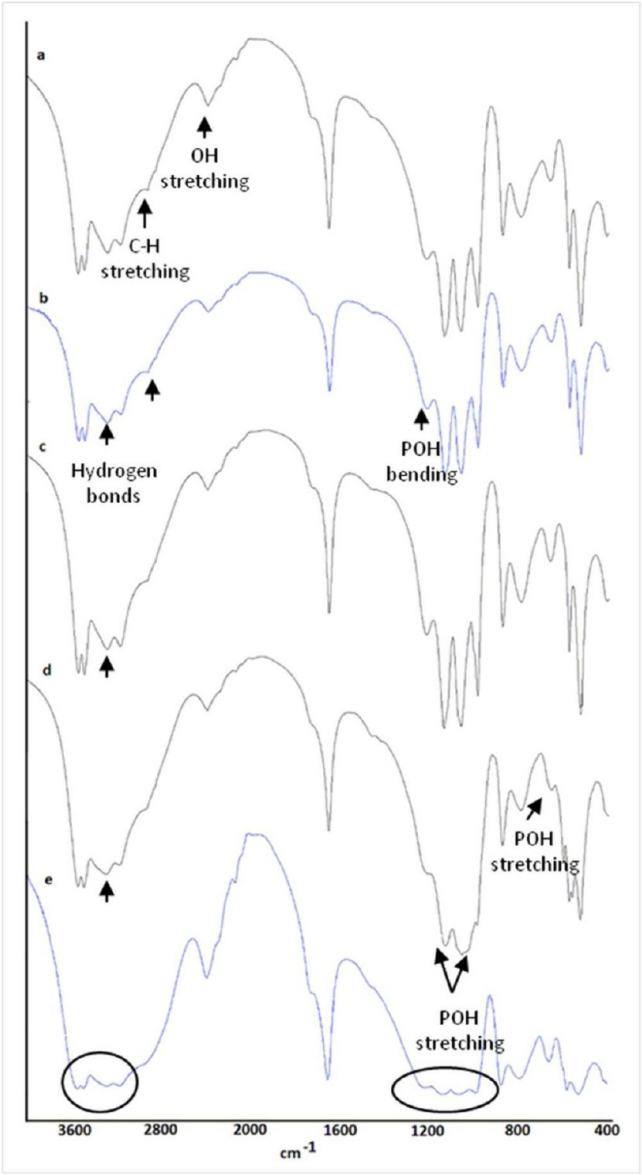

Figure 2. IR spectra of (a) calcium phosphate crystals prepared in 20% starch after diffusion of 0.12 M disodium hydrogen phosphate by a single tube, (b) calcium phosphate crystals prepared in 20% starch after diffusion of 0.19 M calcium chloride by a single tube, (c) calcium phosphate crystals in the U-tube after diffusion of 1.8 M disodium hydrogen phosphate, (d) calcium phosphate crystals in the U-tube after diffusion of 0.8 M disodium hydrogen phosphate, and (e) calcium phosphate crystals in the U-tube after diffusion of 0.2 M disodium hydrogen phosphate.

center (Figure 3c,e). It was reported that pathological brushite precipitates in kidney consist of prismatic needles similar to the morphology and arrangement induced by starch gel (Figure 3f).[38] Meldrum and Cölfen[39] suggested that nucleation in gels generally starts from nanoclusters leading to spherulitic mesocrystals. Kniep and co-workers[40] introduced gelatin as a suitable medium for fluoroapatite growth since gelatin is able to incorporate into the lattices of inorganic crystals to produce fluoroapatite/gelatin composites.

Mineralization of calcium phosphates in U-tubes resulted in three new crystal morphologies consisting of bundled needles to separate aggregates and microcrystals (Figure 3g–n), which are different from the structures produced in single tubes. Highly oriented arrays of needles were grown from the center featuring a diameter of approximately 300 μm (Figure 3i,j). Mineralization of calcium phosphates in starch also presented porous and rough aggregates with a length of around 1 mm (Figure 3k,l). In this regard, the structure of some bundled crystals becomes quite compact (Figure 3m,n), suggesting that starch has a prominent role in nucleation and growth of crystals. The same morphologies of crystals were also reported for brushite crystals precipitated in silica gel.[11−16,41] Plovnick[42] studied the crystallization of brushite using ethylenediaminetetraacetic acid (EDTA) chelated calcium in agar gel. EDTA was offered to control brushite growth rate, size, and morphology in agar compared with direct diffusion controlled reactions. In our previous study on brushite/gelatin composites, we demonstrated that strong interactions between glutamic acid and gelatin macromolecules are able to change the morphology of spherulitic brushite into plate-shaped, mushroom-like, and needle-like crystals.[18]

EDX was used for the analysis of the Ca/P ratio in calcium phosphate crystals (Figure 3). The Ca/P ratio of analytical grade brushite was measured to compare with crystals obtained in starch and found to be 1.14 (RSD = 1%, n = 5). The Ca/P ratios of crystals in starch range from 1.02 to 1.64 (RSD = 1%, n = 5), and the theoretical values of brushite (1.00) and OCP (1.33) are within this range. As it is mentioned later by XRD, only brushite and OCP were found in tubes without any HAp formation after crystallization. This can be due to two reasons: local pH of 4.5 inside starch and lower Ca/P ratios used for synthesis of calcium phosphates in comparison with the one needed for HAp (1.67). For specimens prepared in single tubes, the crystals and aggregates in tube 1 contain less Ca as compared with those in tube 2. Some of the calcium ions in tube 1 are coordinated with starch functional groups in gel, and therefore, they may not bond with phosphate anions after diffusion of 0.12 M disodium hydrogen phosphate to produce calcium phosphate complexes. For specimens prepared in U-tubes, EDX results indicate that the Ca/P ratio is highly dependent on the molarity of ions used. Diffusion of more phosphate anions in tube 3 compared to tube 4 yielded single-crystals with compact needle-like crystals. Also, there is an increased degree of supersaturation of the phosphate ions at the surface, which results in a decrease of the calcium ions concentration in crystals. The changes in Ca/P ratio for porous crystals are in agreement with results of Daniel-da-Silva et al.[43] for κ-carrageenan/HAp composites. An eventual change in the ratio of Ca/P in HAp composites was demonstrated when the polymer/inorganic ratio were higher than 1:1.

X-ray Diffraction Analysis. The X-ray diffraction patterns collected on specimens prepared by the single-diffusion (tubes 1 and 2) and double-diffusion (tubes 3–5) methods are illustrated in Figure 4.

As shown in Figure 4, the single-diffusion method led to the formation of single-phase monoclinic brushite (calcium phosphate hydroxide hydrate, space group *Cc*(9), PDF 9-077) in both specimens (tubes 1 and 2). This indicates that the relative concentration of the $CaCl_2$ and Na_2HPO_4 reactants is the dominant factor in determining the nature of the synthesized nanocrystals. However, small differences between the intensity ratios of the low-angle diffraction lines in crystals in tubes 1 and 2 suggest that different degrees of texture (preferential orientation) might exist. This effect could correlate with the lower Ca-content in the nanocrystals and aggregates of tube 1 compared to tube 2.

dx.doi.org/10.1021/cg4002434 | *Cryst. Growth Des.* 2013, 13, 2166–2173

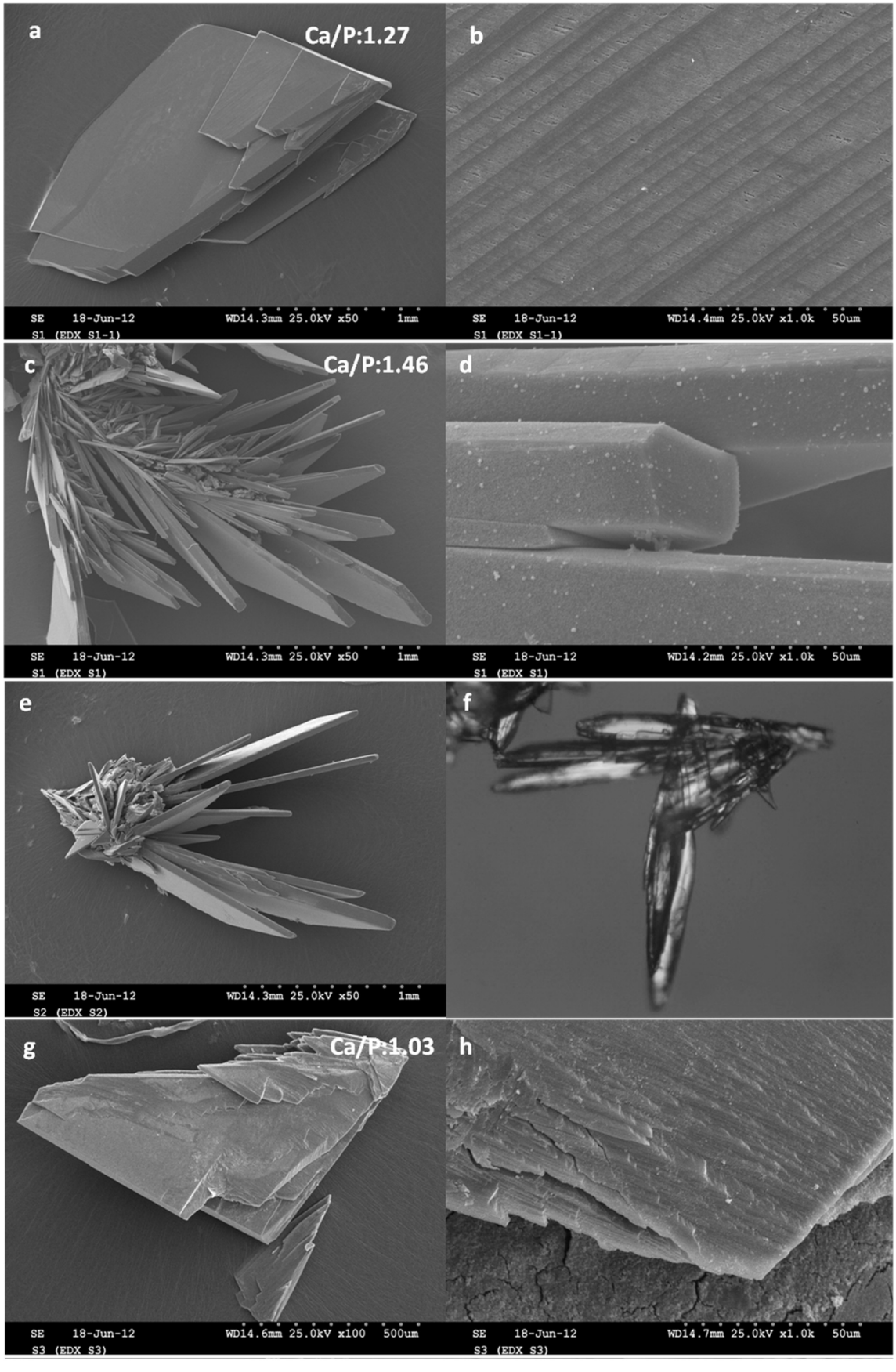

Figure 3. continued

dx.doi.org/10.1021/cg4002434 | *Cryst. Growth Des.* 2013, 13, 2166−2173

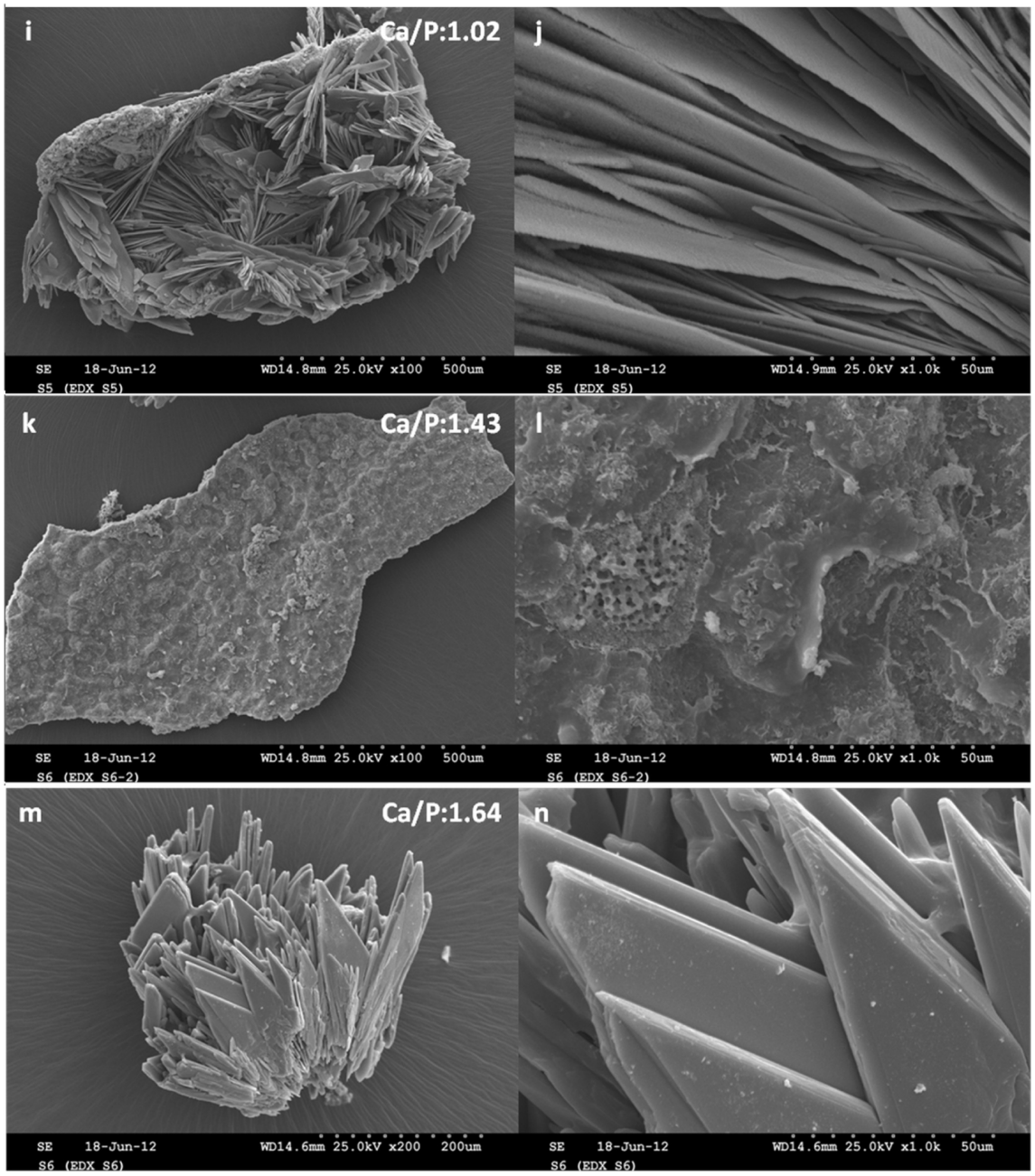

Figure 3. SEM images of calcium phosphate crystals obtained in single and U-tube (a–d) crystals prepared in single tube 1 and (e) crystals prepared in single tube 2. (f) Pathological brushite found in kidney, photo provided by Louis C. Herring and Co., a recognized world leader in kidney stone analysis. (g,h) Crystals prepared in U-tube 3, (i,j) crystals prepared in U-tube 4, and (k–n) crystals prepared in U-tube 5.

The single-phase monoclinic brushite phase is also obtained by the double-diffusion technique for a precursor $CaCl_2$/Na_2HPO_4 molar ratio equal to 1/1.8 (sample in tube 3, Table 2). By decreasing the concentration of Na phosphate precursor (tube 4), the formation (~15%) of triclinic octacalcium phosphate (OCP, space group $P\bar{1}(2)$, PDF 26-1056) as the secondary phase is supported (Figure 4). At equimolar concentrations of the precursor phases (tube 5), the amount of secondary OCP phase raises up to approximately 36% (Table 2).

Grain sizes were estimated from the widths of the strongest Bragg diffraction lines of the brushite and OCP constituent phases as mentioned earlier (Table 2). It can be recognized that, for brushite, the average crystallite sizes are close to approximately 60 (±3) nm irrespective of the preparation method employed. This further implies a linear growth rate of brushite nanocrystals near to 20 nm per week. In contrast, the average crystallite sizes of the OCP phase differ significantly between the tubes 4 and 5, which demonstrates a faster growth of the OCP and thus an improved OCP crystallinity at equimolar concentration of the $CaCl_2$/Na_2HPO_4 precursors (tube 5), as also clearly shown in Figure 4.

Observation of Starch Inclusion by Confocal Laser Scanning Microscopy. Demineralization of crystals grown in some tubes was performed by EDTA in order to measure the amount of starch inclusion in crystals. About 1.5% starch was found in our brushite samples similar to the gelatin content in a fluorapatite/gelatin composite (2.3%)[40] and the protein

dx.doi.org/10.1021/cg4002434 | Cryst. Growth Des. 2013, 13, 2166–2173

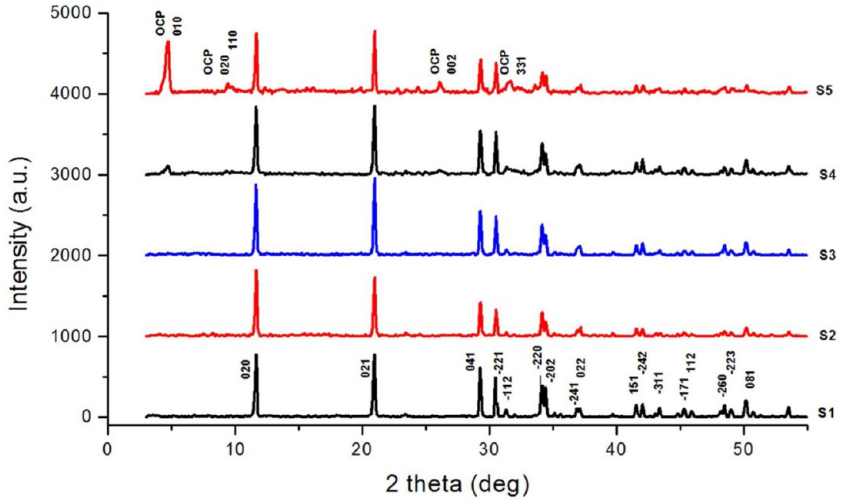

Figure 4. X-ray diffraction patterns collected on specimen tubes 1−5.

Table 2. Grain Size and the Refined Cell Parameters for the Samples 1−5

sample tube	grain size (nm)	cell parameters a,b,c (Å)	cell parameters α, β, γ (deg)	phase fraction (%)
1	(B[a]) G_{020} = 58.62	(B) a = 6.3617(12)	(B) $\alpha = \gamma = 90$	(B) 100
	G_{021} = 61.36	b = 15.1751(21)	β = 118.512(11)	
		c = 5.8116(9)		
2	(B) G_{020} = 65.34	(B) a = 6.3581(11)	(B) $\alpha = \gamma = 90$	(B) 100
	G_{021} = 62.22	b = 15.1687(20)	β = 118.500(11)	
		c = 5.8090(9)		
3	(B) G_{020} = 56.95	(B) a = 6.3591(8)	(B) $\alpha = \gamma = 90$	(B) 100
	G_{021} = 61.70	b = 15.1713(15)	β = 118.517(8)	
		c = 5.8084(7)		
4		(B) a = 6.3586(12)	(B) $\alpha = \gamma = 90$	
	(B) G_{020} = 54.77	b = 15.1758(23)	β = 118.510(11)	(B) 85.008
	G_{021} = 61.95	c = 5.8103(9)		
	(OCP)	(OCP)	(OCP)	(OCP) 14.992
	G_{010} = 21.49	a = 9.5193(26)	α = 93.187(29)	
		b = 19.0300(46)	γ = 90.040(28)	
		c = 6.8460(20)	β = 79.637(27)	
5		(B) a = 6.3572(21)	(B) $\alpha = \gamma = 90$	
	(B) G_{020} = 63.15	b = 15.1636(44)	β = 118.508(20)	(B) 64.16
	G_{021} = 64.58	c = 5.8106(17)		
	(OCP)	(OCP)	(OCP)	(OCP) 35.84
	G_{010} = 35.27	a = 9.5011(31)	α =92.496(43)	
		b = 19.0140(97)	γ = 90.107(39)	
		c = 6.8308(26)	β = 79.923(31)	

[a]B: brushite.

content of brushite kidney stones (4.1 ± 1.6%).[44] Laser scanning was carried out in different layers of crystals featuring starch inclusion in calcium phosphates, and the result is shown in Figure 5. It can be seen that the structure is developed by starch precursors for consecutive complex formation at the growth front.

As stated earlier, starch gel is formed by amylose and amylopectin through hydrogen bonds with water as a bridging molecule. In this regard, the energy states of amylose molecules are lowered, tending to form lamellar crystalline arrays of hexagonally packed double helices. Highly branched amylopectin with very large molecular weight thus consists of alternating crystalline and amorphous lamellae.[45−47] Both amylose and amylopectin are cross-linked together to form rigid junction zones and mobile amorphous interjunction

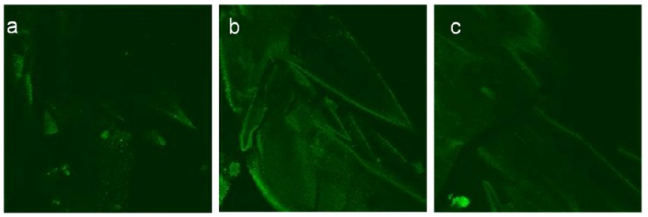

Figure 5. Pyranine stained starch in calcium phosphate crystals as scanned by a microscope after excitation: (a) upper layer of stained crystal, (b) inner layer of stained crystal, and (c) lower layer of stained crystal.

segments due to interchain associations in gel.[48,49] Two factors affect the crystallization in starch: functional groups acting as

dx.doi.org/10.1021/cg4002434 | Cryst. Growth Des. 2013, 13, 2166−2173

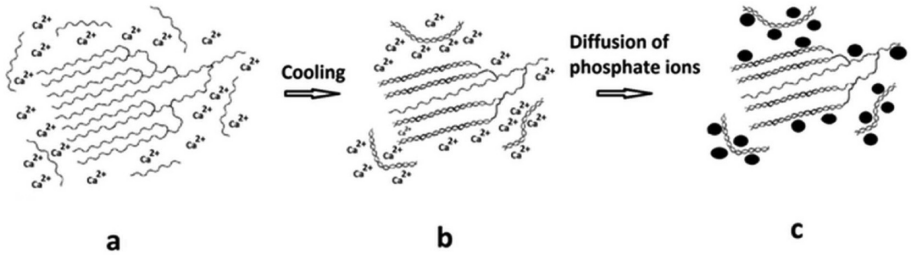

Figure 6. Mechanism of calcium phosphate formation in starch gel: (a) amylose and amylopectin molecules in the presence of calcium ions, (b) formation of double helices and starch gelation after cooling in the presence of calcium ions, and (c) formation of calcium phosphate nuclei after diffusion of phosphate ions in starch gel.

nucleators and gel porosity. Starch presents a surface negative charge above pH 3.7. This results in the establishment of an electrical double layer that mediates electrostatic interactions with calcium ions.[50] A stereochemical match of hydroxyl groups to calcium ions parallel to the direction of right handed helices is further required for changing the surface energy in crystallization.[49] The internal pores present in gel also act as nucleation sites depending on the ionic concentration and degree of supersaturation of the Ca and P ions diffused inside the pores. After the diffusion of phosphate anions, they can react with Ca^{2+} cations in pores to form calcium phosphate nuclei. Hydrogen bonds are further formed among the helical molecule chains of starch gel and calcium phosphate nuclei to obtain heterogeneous precipitation of large needles.[51,52] Previous investigations for preparation of HAp/starch composites showed that the electrostatic and hydrogen bindings of hydroxyl groups of starch on one hand and calcium ions on the other hand are the key factors for the nucleation and growth of HAp.[23] Iafisco et al.[16] observed large channels and pores in brushite synthesized in silica gel after the alkaline dissolution of silica. Silica was found intercalated among perfectly aligned crystalline domains of OCP. Moreover, it was revealed that proteins and keratin entered to crystalline brushite could play an important role in regulating the arrangement of brushite precipitated from human urine.[38,44] A detailed study of the mechanism of nucleation and growth of needle-like calcium phosphate crystals in starch may provide helpful information on the mineralization of brushite kidney stones. This is consistent with our present EDX and IR results. Figure 6 illustrates the proposed mechanism for calcium phosphate formation in starch gel.

SUMMARY AND CONCLUSIONS

This work was carried out to study the effect of starch gel on calcium phosphate crystal growth. IR spectroscopy analysis demonstrated the functionality of starch nucleators to interact strongly with calcium and phosphate ions in order to produce brushite and OCP crystal composites. The backbone of starch matrix with hydroxyl functional groups provided a template for the nucleation and growth of calcium phosphate crystals. In this regard, the macromolecular conformation of amylase and amylopectin in the presence of calcium and phosphate ions induced crystalline calcium phosphate/starch composites. This promoted two types of morphologies including microscale platelets and bundled needles. Such crystal shapes bear strong resemblance to brushite kidney stones. The investigation of calcium phosphate crystallization in starch therefore provides a new guideline for studying the mechanism of kidney stone growth.

AUTHOR INFORMATION

Corresponding Author

*E-mail: mparvinzadeh@gmail.com or mazeyar.parvinzadeh@dcb.unibe.ch (M.P.G.); juerg.hulliger@iac.unibe.ch (J.H.).

Notes

The authors declare no competing financial interest.

ACKNOWLEDGMENTS

We thank Beatrice Frey for providing SEM images. Furthermore, we would like to acknowledge Matthias Burgener for assistance with the optical microscopy.

REFERENCES

(1) Buléon, A.; Colonna, P.; Planchot, V.; Ball, S. *Int. J. Biol. Macromol.* **1998**, *23*, 85−112.
(2) Sajilata, M. G.; Singhal, R. S.; Kulkarni, P. R. *Compr. Rev. Food Sci. Food Saf.* **2006**, *5*, 1−17.
(3) Tako, M.; Hizukuri, S. *Carbohydr. Polym.* **2002**, *48*, 397−401.
(4) Rubens, P.; Snauwaert, J.; Heremans, K.; Stute, R. *Carbohydr. Polym.* **1999**, *39*, 231−235.
(5) Dorozhkin, S. V. *Biomaterials* **2010**, *31*, 1465−1485.
(6) Tamimi, F.; Sheikh, Z.; Barralet, J. *Acta Biomater.* **2012**, *8*, 474−487.
(7) Bose, S.; Tarafder, S. *Acta Biomater.* **2012**, *8*, 1401−1421.
(8) Schweizer, S.; Taubert, A. *Macromol. Biosci.* **2007**, *7*, 1085−1099.
(9) De Yoreo, J. J.; Wierzbicki, A.; Dove, P. M. *Cryst. Eng. Comm.* **2007**, *9*, 1144−1152.
(10) Gorna, K.; Muñoz-Espí, R.; Gröhn, F.; Wegner, G. *Macromol. Biosci.* **2007**, *7*, 163−73.
(11) LeGeros, R. Z.; LeGeros, J. P. *J. Cryst. Growth* **1972**, *13−14*, 476−480.
(12) Ohta, M.; Tsutsumi, M.; Ueno, S. *J. Cryst. Growth* **1979**, *47*, 135−136.
(13) Ohta, M.; Tsutsumi, M. *J. Cryst. Growth* **1982**, *56*, 652−658.
(14) Sokołowski, T.; Wiktorowska, B. *Cryst. Res. Technol.* **1990**, *25*, 481−487.
(15) Rajendran, K.; Keefe, C. D. *Cryst. Res. Technol.* **2010**, *45*, 939−945.
(16) Iafisco, M.; Marchetti, M.; Morales, J. G.; Hernández-Hernández, M. A.; Ruiz, J. M. G.; Roveri, N. *Cryst. Growth Des.* **2009**, *9*, 4912−4921.
(17) Furuichi, K.; Oaki, Y.; Imai, H. *Chem. Mater.* **2006**, *18*, 229−234.
(18) Parvinzadeh Gashti, M.; Bourquin, M.; Stir, M.; Hulliger, J. *J. Mater. Chem. B* **2013**, *1*, 1501−1508.
(19) Lemos, A. F.; Ferreira, J. M. F. *Mater. Sci. Eng., C* **2000**, *11*, 35−40.
(20) Marques, A. P.; Reis, R. L. *Mater. Sci. Eng., C* **2005**, *25*, 215−229.
(21) Xiang, J.; Cao, H.; Warner, J. H.; Watt, A. R. *Cryst. Growth Des.* **2008**, *8*, 4583−4588.

(22) Kundu, A.; Lemos, A.; Soundrapandian, C.; Sen, P. S.; Datta, S.; Ferreira, J. M. F.; Basu, D. *J. Mater. Sci.: Mater. Med.* **2010**, *21*, 2955−2969.
(23) Sadjadi, M. S.; Meskinfam, M.; Sadjadi, B.; Jazdarreh, H.; Zare, K. *Mater. Chem. Phys.* **2010**, *124*, 217−222.
(24) Meskinfam, M.; Sadjadi, M. A. S.; Jazdarreh, H.; Zare, K. *J. Biomed. Nanotechnol.* **2011**, *7*, 455−459.
(25) Sundaram, J.; Durance, T. D.; Wang, R. *Acta Biomater.* **2008**, *4*, 932−942.
(26) Jaya, S.; Durance, T. D.; Wang, R. *J. Compos. Mater.* **2009**, *43*, 1451−1460.
(27) Raafat, A. I.; Eidin, A. A. S.; Salama, A. A.; Ali, N. S. *J. Appl. Polym. Sci.* **2013**, *128*, 1697−1705.
(28) McGrane, S. J.; Mainwaring, D. E.; Cornell, H. J.; Rix, C. J. *Starch/Stärke* **2004**, *56*, 122−131.
(29) Parvinzadeh, M.; Moradian, S.; Rashidi, A.; Yazdanshenas, M. E. *Appl. Surf. Sci.* **2010**, *256*, 2792−2802.
(30) Parvinzadeh, M.; Moradian, S.; Rashidi, A.; Yazdanshenas, M. E. *Polym.-Plast. Technol. Eng.* **2010**, *49*, 874−884.
(31) Parvinzadeh Gashti, M.; Eslami, S. *Superlattices Microstruct.* **2012**, *51*, 135−148.
(32) Parvinzadeh Gashti, M.; Alimohammadi, F.; Shamei, A. *Surf. Coat. Technol.* **2012**, *206*, 3208−3215.
(33) Parvinzadeh Gashti, M.; Pournaserani, A.; Ehsani, H.; Parvinzadeh Gashti, M. *Vacuum* **2013**, *91*, 7−13.
(34) Xie, J.; Riley, C.; Kumar, M.; Chittur, K. *Biomaterials* **2002**, *23*, 3609−3616.
(35) Štulajterová, R.; Medvecký, L. *Colloid. Surf., A* **2008**, *316*, 104−109.
(36) Temizel, N.; Girisken, G.; Tas, A. C. *Mater. Sci. Eng., C* **2011**, *31*, 1136−1143.
(37) Monma, H.; Kamiya, T. *J. Mater. Sci.* **1987**, *22*, 4247−4250.
(38) Thurgood, L. A.; Ryall, R. L. *J. Proteome Res.* **2010**, *9*, 5402−5412.
(39) Meldrum, F. C.; Cölfen, H. *Chem. Rev.* **2008**, *108*, 4332−432.
(40) Busch, S.; Schwarz, U.; Kniep, R. *Adv. Funct. Mater.* **2003**, *13*, 189−198.
(41) Pereira, M. M.; Hench, L. L. *J. Sol-Gel. Sci. Technol.* **1996**, *7*, 59−68.
(42) Plovnick, R. H. *J. Cryst. Growth* **1991**, *114*, 22−26.
(43) Daniel-da-Silva, A. L.; Lopes, A. B.; Gil, A. M.; Correia, R. N. *J. Mater. Sci.* **2007**, *42*, 8581−8591.
(44) Pramanik, R.; Asplin, J. R.; Jackson, M. E.; Williams, J. C., Jr. *Urol. Res.* **2008**, *36*, 251−258.
(45) Veelaert, S.; de Wita, D.; Gotlieb, K. F.; Verhé, R. *Carbohydr. Polym.* **1997**, *32*, 131−139.
(46) Mohammed, Z. H.; Hember, M. W. N.; Richardson, R. K.; Morris, E. R. *Carbohydr. Polym.* **1998**, *36*, 37−48.
(47) BeMiller, J. N. *Carbohydr. Polym.* **2011**, *86*, 386−423.
(48) Evagelioua, V.; Richardsona, R. K.; Morris, E. R. *Carbohydr. Polym.* **2000**, *42*, 261−272.
(49) Richardson, G.; Sun, Y.; Langton, M.; Hermansson, A. M. *Carbohydr. Polym.* **2004**, *57*, 369−377.
(50) Marsh, R. A.; Waight, S. G. *Starch/Stärke* **1982**, *34*, 149−152.
(51) Montero, P.; Pérez-Mateos, M. *Food Hydrocolloids* **2002**, *16*, 375−385.
(52) Yuguchi, Y.; Urakawa, H.; Kajiwara, K. *Food Hydrocolloids* **2003**, *17*, 481−485.